

# Boosting Adversarial Transferability with Spatial Adversarial Alignment

Zhaoyu Chen<sup>1\*</sup>, Haijing Guo<sup>1\*</sup>, Kaixun Jiang<sup>1</sup>, Jiyuan Fu<sup>1</sup>, Xinyu Zhou<sup>1</sup>,  
Dingkang Yang<sup>1</sup>, Hao Tang<sup>2</sup>, Bo Li<sup>3</sup>, Wenqiang Zhang<sup>1†</sup>

<sup>1</sup>Fudan University <sup>2</sup>Peking University <sup>3</sup>vivo Mobile Communication Co.

zhaoyuchen20@fudan.edu.cn, hjguo22@m.fudan.edu.cn, wqzhang@fudan.edu.cn

## Abstract

*Deep neural networks are vulnerable to adversarial examples that exhibit transferability across various models. Numerous approaches are proposed to enhance the transferability of adversarial examples, including advanced optimization, data augmentation, and model modifications. However, these methods still show limited transferability, particularly in cross-architecture scenarios, such as from CNN to ViT. To achieve high transferability, we propose a technique termed Spatial Adversarial Alignment (SAA), which employs an alignment loss and leverages a witness model to fine-tune the surrogate model. Specifically, SAA consists of two key parts: spatial-aware alignment and adversarial-aware alignment. First, we minimize the divergences of features between the two models in both global and local regions, facilitating spatial alignment. Second, we introduce a self-adversarial strategy that leverages adversarial examples to impose further constraints, aligning features from an adversarial perspective. Through this alignment, the surrogate model is trained to concentrate on the common features extracted by the witness model. This facilitates adversarial attacks on these shared features, thereby yielding perturbations that exhibit enhanced transferability. Extensive experiments on various architectures on ImageNet show that aligned surrogate models based on SAA can provide higher transferable adversarial examples, especially in cross-architecture attacks.*

## 1. Introduction

Deep neural networks (DNNs) have been successfully and extensively deployed across security-sensitive applications, including autonomous driving [46, 50, 51], facial verification [34, 52, 53], and video surveillance [14, 17, 18, 54]. However, DNNs exhibit considerable vulnerability to adversarial examples [3–6, 12, 13, 27], where imperceptible

perturbations are introduced into natural images, leading models to produce incorrect predictions. In real-world applications, DNNs are typically concealed from user access, necessitating adversaries to generate adversarial examples within a black-box setting, where no knowledge of the target model’s parameters or architecture is available. Adversarial transferability plays a crucial role in black-box settings as it allows adversaries to effectively compromise target models by employing adversarial examples generated on surrogate models. In black-box settings, adversarial transferability plays a crucial role, which enables adversaries to leverage adversarial examples crafted on surrogate models to effectively attack target models. Thus, generating highly transferable adversarial examples is instrumental in uncovering and understanding the vulnerabilities within DNNs, drawing substantial attention in recent research.

Cross-model transferability has been extensively studied for CNNs [9, 10, 45]. Highly transferable adversarial examples are usually based on advanced optimization [9, 22, 37] and data augmentation [10, 25, 45]. The principle is to alleviate the overfitting of adversarial examples on surrogate models, determining whether the attack can be successfully transferred to the target models. In addition, some model modification methods [15, 44], such as amplifying the gradient on skip connections (the structure in ResNet [16]), can also improve transferability. However, few works explore adversarial transferability on Vision Transformer (ViT) [11] and the performance of existing work extending CNN to ViT is poor due to significant structural differences. Specifically, ViT flattens the image into a sequence of patch tokens and employs multi-head self-attention to capture global relationships among the patches. In contrast, CNNs typically consist of stacked convolutional layers that learn feature relationships progressively through downsampling. Therefore, [43] first empirically analyzes the structure of ViT and propose PNA and PatchOut [43], but there is still much room for improvement in cross-architecture transferability.

In this paper, we argue that unique structural features are critical to cross-architecture adversarial transferability. Given a dataset, various models tend to exhibit analogous

\*indicates equal contributions.

†indicates corresponding author.

decision boundaries [23], arising from their ability to learn similar features. If we can obtain a surrogate model whose features are similar to those of models with different architectures, then the resulting adversarial perturbation can be transferable across different models. A recent technique known as Model Alignment (MA) [26] employs an alignment loss to minimize prediction divergences between surrogate models and witness models, thereby indirectly facilitating the extraction of features that are similarly represented by the witness model. However, directly applying MA to black-box attacks may lead to the degradation of cross-architecture transferability. The main reasons are: (i) Features are not aligned in space. MA only uses the final prediction of the model, but in fact, the spatial features of ViT and CNN are different. It is difficult to directly constrain the similarity of features only by the final logits. (ii) Features are not aligned from the perspective of adversarial features. In addition to the features of clean images, the features of adversarial examples also have similarities across different models and need to be considered.

To overcome these challenges and enhance transferability, we propose a technique called Spatial Adversarial Alignment (SAA), which utilizes an alignment loss from the perspective of spatial and adversarial features and incorporates a witness model to refine the surrogate model. SAA consists of two key parts: spatial-aware alignment and adversarial-aware alignment. In the spatial-aware alignment, in addition to aligning on the final global features, we also focus on the features of local regions. We make local features of CNNs by position to align ViTs’ embeddings at the same position. In the adversarial-aware alignment, we introduce a self-adversarial strategy, which constructs adversarial examples so that the model can learn the differences between different architectures in adversarial features, thereby enabling the model to further capture more common features. Aligned surrogate models by SAA provide promising adversarial transferability and can be seamlessly integrated with existing transfer attacks. Our contributions can be summarized as follows:

- We reveal for the first time the importance of spatial and adversarial features for cross-architecture transferability.
- We propose Spatial Adversarial Alignment (SAA), which leverages a witness model to fine-tune the surrogate model via spatial-aware and adversarial-aware alignment to generate highly transferable adversarial examples.
- Experiments on 6 CNNs and 4 ViTs show that SAA has state-of-the-art adversarial transferability, especially in cross-model transferability. Compared with MA, on ResNet50, the transferability from CNN to ViT is improved by 25.5-39.1%.

## 2. Related Work

### 2.1. Transfer attacks on CNNs

Early transfer attacks are mainly conducted between CNNs, and the most popular methods were advanced optimization [9, 22, 37], data augmentation [10, 25, 45], and model modification [15, 43, 44].

**Advanced Optimization.** [22] compare adversarial attacks to model training: better optimization methods can obtain models with better generalization, and therefore also generate adversarial examples with higher transferability. FGSM [13] is the earliest gradient-based transfer attack, which was then extended to I-FGSM [20]. The subsequent advance optimization further improves the transferability by introducing momentum [9, 22, 37, 39] and smoothness [31].

**Data Augmentation.** Data augmentation serves as an effective strategy to prevent model overfitting, achieving state-of-the-art performance in model generalization [8, 48]. Building on this principle, numerous adversarial attacks incorporate various transformations to enhance adversarial transferability, including modifications in size [45], scale [22], mixup [40], and frequency domain [25] adjustments. This integration aims to mitigate the overfitting of adversarial examples to the surrogate model, thereby increasing their effectiveness across different models.

**Model Modification.** According to certain characteristics of the model, modifying the parameters of the surrogate model or changing the forward or backward propagation can also improve the transferability. Skip Gradient Method (SGM) [44] using more gradients from the skip connections rather than the residual modules, allows one to craft adversarial examples with high transferability. Similarly, Linear Backpropagation (LinBP) [15] and Backward Propagation Attack (BPA) [41] concentrate on non-linear activations by modifying the ReLU derivatives to enhance attack transferability. Model Alignment (MA) [26] promotes alignment of model predictions through an alignment loss relative to a witness model, with the aim of capturing shared features across models. However, MA overlooks spatial and adversarial feature alignment across architectures, limiting its effectiveness. Unlike these methods, our SAA requires no modifications to the forward or backpropagation processes, enabling the efficient generation of highly transferable adversarial examples with minimal training overhead. In contrast, LinBP and BPA, involve altering backpropagation or even full model retraining, incurring significantly higher computational costs.

### 2.2. Transfer attacks on ViTs

Current transfer attacks for ViTs largely adapt methods developed for CNNs. Pay No Attention (PNA) [43] method extends Skip Gradient Method (SGM) to ViTs by omitting the gradient computation of attention blocks during

back-propagation, thereby enhancing adversarial transferability. PatchOut [43] strategy selects a random subset of image patches to compute the gradient at each iteration, functioning as an image transformation technique to increase transferability. Then, Self-Ensemble (SE) [29] approach employs the class token at each layer with a shared classification head to create an ensemble model, facilitating optimized perturbation; however, many ViTs, such as Visformer [2] and CaiT [36], lack sufficient class tokens to build this ensemble. Additionally, Token Refinement (TR) [29] module fine-tunes class tokens to further boost transferability. Recently, Token Gradient Regularization (TGR) [49] works from the perspective of variance reduction, stabilizing the gradient direction to prevent adversarial examples from getting stuck in poor local optima. Distinct from these approaches, SAA is the first method to specifically analyze architectural differences across models. By leveraging shared features between different architectures, SAA enables the creation of more generalized surrogate models that integrate seamlessly with optimization and data augmentation methods, ultimately achieving state-of-the-art transferability.

### 3. Methodology

#### 3.1. Preliminaries

In this paper, we focus on the image classification task on DNNs. Let  $f_\theta(\cdot)$  represent a DNN-based classifier with parameters  $\theta$ . We denote the clean image as  $x$  and its corresponding ground-truth label as  $y$ . Following [9, 10, 45], we evaluate the adversarial transferability under untargeted adversarial attacks with  $l_\infty$  norm. Therefore, the goal of transfer attacks is to add an adversarial perturbation to the clean image  $x$  based on the information of the surrogate model  $f_{\theta_s}(\cdot)$  to obtain the adversarial example  $x_{adv}$ , so that  $f_{\theta_s}(x_{adv}) \neq y$  subject to the constraint that  $\|x_{adv} - x\|_\infty \leq \epsilon$ . In the black-box setting, no information about the target model—such as its architecture, weights, or gradients—is accessible. Therefore, adversarial examples are generated solely by utilizing a surrogate model  $f_{\theta_s}(\cdot)$ , leveraging their transferability to deceive the target model  $f_{\theta_t}(\cdot)$ .

#### 3.2. Spatial Adversarial Alignment (SAA)

Spatial Adversarial Alignment (SAA) employs an alignment loss tailored to both spatial and adversarial feature perspectives, incorporating a witness model to fine-tune the surrogate model. SAA aims to adjust the surrogate model to extract features closely aligned with those of the witness model, capturing both spatial and adversarial features shared across models. As shown in Figure 1, SAA consists of two parts, namely spatial-aware alignment and adversarial-aware alignment.

**Spatial-aware Alignment.** The purpose of spatial-aware

alignment is to make the surrogate and witness models more consistent in the feature space. Naturally, the most intuitive approach to aligning the feature distributions of two models is to minimize the distance between their final outputs. However, when the models exhibit significant architectural differences, ensuring output similarity alone is insufficient to achieve alignment in intermediate features. In black-box attacks, where the details of the target model’s architecture are unknown, this issue becomes more pronounced. Taking the challenging scenario of CNN to ViT as an example, their intermediate layer features differ substantially in semantic levels. This discrepancy arises primarily from differences in receptive fields, stacking methodologies, and normalization techniques between CNNs and ViTs. Therefore, relying solely on output alignment for model fine-tuning indirectly captures some common features, but this approach can, in certain cases, result in degraded transferability, as observed in methods like Model Alignment (MA) [26].

Therefore, in addition to aligning on the final global features, we also need focus on the features of local regions. For ease of understanding, we define the global features  $f_\theta(x)$  as the logits of the model corresponding to the input  $x$ . For CNNs, it is the output of features by the last layer. For ViTs, it refers to the final embedding of the [CLS] token after the MLP block. First, we perform alignment at the global feature level by defining an alignment loss between the surrogate model and witness model at the output layer:

$$\mathcal{L}_{global}(x; \theta_s) = D_{KL}(f_{\theta_s}(x), f_{\theta_w}(x)), \quad (1)$$

where  $D_{KL}$  measures the feature divergence with Kullback-Leibler (KL) divergence.

Next, we align the models at the local feature level. Here, we define  $z_\theta(x)$  as local features. For CNNs,  $z_\theta(x)^{B \times C \times H \times W}$  is the features of the last layer before passing through the global average pooling layer. For ViTs,  $z_\theta(x)^{B \times C' \times H \times W^*}$  is the embeddings of the patch tokens after passing through the MLP except for the [CLS] token, where each patch token corresponds to a specific spatial region in the input. Each spatial position  $(h, w)$  within this feature map is treated as a distinct local region and the feature for each local region is  $z_\theta^{[q]}(x)$ , where  $q = \{1, 2, \dots, H \times W\}$ . Let  $z_{\theta_s}^{[q]}(x)$  and  $z_{\theta_w}^{[q]}(x)$  denote the local prediction (logits) associated with each local region  $q$  for the surrogate model and witness model, respectively. Next, we compute the pseudo-labels of the local region  $q$  based on the local features of the witness models. We denote this pseudo-label as  $\hat{y}_{\theta_w}^{[q]}$ , which is obtained by taking the arg max over the logits from the witness model:  $\hat{y}_{\theta_w}^{[q]} = \arg \max(f_{\theta_w}(z_{\theta_w}^{[q]}(x)))$ . Then, we use this pseudo-label to supervise the learning of the local feature of the

\*Generally, ViT’s patch embeddings  $z(x)$  is  $(B, N, C')$  by default. We first transform it to  $(B, C', H', W')$ , where  $N = H' \times W'$ . Then, we perform an adaptive pooling operation to transform it to  $(B, C', H, W)$ .

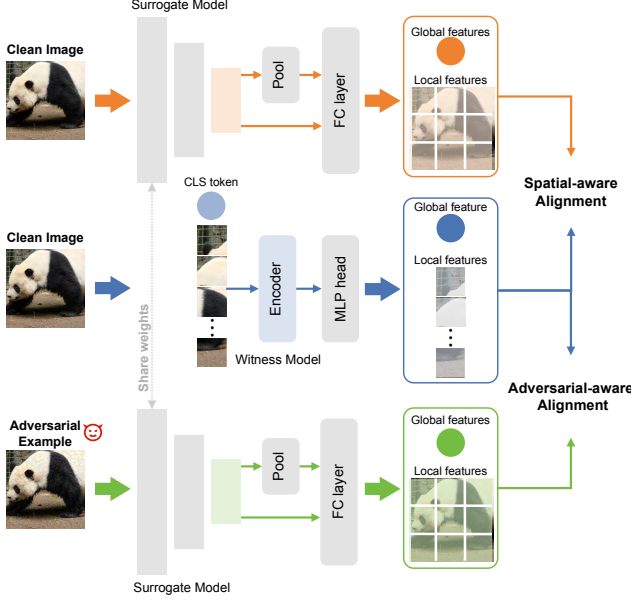


Figure 1. Spatial Adversarial Alignment (SAA) consists of two parts: spatial-aware alignment and adversarial-aware alignment. Initially, we aim to minimize the feature divergences between the two models across both global and local regions, thereby promoting spatial alignment. Subsequently, we introduce a self-adversarial strategy that utilizes adversarial examples to impose additional constraints, aligning the adversarial features.

surrogate model. To achieve local alignment, we minimize the divergence between the logits of corresponding local regions, so the local alignment loss is expressed as:

$$\mathcal{L}_{local}(x; \theta_s) = \frac{1}{HW} \sum_{q=1}^{HW} D_{CE}(z_{\theta_s}^{[q]}(x), \arg \max(f_{\theta_w}(z_{\theta_w}^{[q]}(x)))) \quad (2)$$

where  $D_{CE}$  is the cross-entropy loss. Therefore, the spatial-aware alignment loss is expressed as:

$$\mathcal{L}_{SA}(x; \theta_s) = \mathcal{L}_{global}(x; \theta_s) + \gamma \cdot \mathcal{L}_{local}(x; \theta_s), \quad (3)$$

where  $\gamma$  is the spatial factor. By minimizing this spatial-aware alignment loss, we encourage the surrogate model to produce features in both global and local regions that are consistent with those of the witness model, even across different architectures.

**Adversarial-aware Alignment.** The relationship between features and adversarial vulnerability is highly significant. Some hypotheses [30, 47] propose that adversarial examples possess distinct feature distributions compared to normal examples, which may inherently predispose models to adversarial vulnerability—a notion supported by several studies [1, 25]. Beyond normal examples, learning adversarial features may offer a way to capture shared features between surrogate models and witness models. Furthermore, [10] suggests that models trained with adversarial

examples focus on more discriminative regions within images, displaying feature recognition patterns distinct from those of normally trained models. Thus, adversarial examples play a crucial role in achieving model alignment.

In our adversarial-aware alignment, we introduce a self-adversarial strategy that constructs adversarial examples of the surrogate model to enable the model to discern architectural differences in adversarial features effectively. Specifically, we leverage the gradients to iteratively generate adversarial examples under the supervision of the global features of the witness model. Assuming  $x_{adv}^{(0)} = x$ , we define the adversarial example  $x_{adv}^{(t+1)}$  of the surrogate model as:

$$x_{adv}^{(t+1)} = \Pi_{x, \epsilon} \left( x_{adv}^{(t)} + \alpha \cdot \text{sign} \left( \nabla_x D_{KL} \left( f_{\theta_s}(x_{adv}^{(t)}), f_{\theta_w}(x) \right) \right) \right), \quad (4)$$

where  $D_{KL}$  denotes the KL divergence,  $x_{adv}^{(t)}$  denotes the adversarial example at iteration  $t$ ,  $\alpha$  is the step size, and  $\Pi_{\epsilon}$  projects the adversarial example onto an  $\epsilon$ -bounded neighborhood around the original input  $x$ .

Once the adversarial example  $x_{adv}$  is generated, we also perform adversarial-aware alignment on the adversarial examples from global and local features to further align the surrogate and witness models. The loss of the adversarial-aware alignment is expressed as:

$$\mathcal{L}_{AA}(x_{adv}; \theta_s) = \mathcal{L}_{global}(x_{adv}; \theta_s) + \omega \cdot \mathcal{L}_{local}(x_{adv}; \theta_s), \quad (5)$$

where  $\omega$  is the adversarial factor.

**Optimization.** Combining spatial-aware and adversarial-aware alignment, the final optimization goal of spatial-adversarial alignment is:

$$\mathcal{L}_{SAA}(x; \theta_s) = \mathcal{L}_{SA}(x; \theta_s) + \kappa \cdot \mathcal{L}_{AA}(x_{adv}; \theta_s), \quad (6)$$

where  $\kappa$  is the alignment factor to balance the two alignments. If not otherwise stated, we define  $\gamma = 0.2$ ,  $\omega = 0.02$ , and  $\kappa = 0.02$  in this paper.

Spatial-adversarial alignment facilitates the alignment of the surrogate model with a collection of witness models to further improve the adversarial transferability. This process involves utilizing a set of witness models, denoted as  $\Theta$ , where the cardinality of the set is represented by  $|\Theta|$ . Therefore, the parameter update rule for the surrogate model, based on stochastic gradient descent (SGD), can be expressed as follows:

$$\theta_s^{(t+1)} = \theta_s^{(t)} - \eta \cdot \frac{1}{|\mathcal{B}||\Theta|} \sum_{x \in \mathcal{B}} \sum_{\theta_w \in \Theta} \nabla_{\theta_s^{(t)}} \mathcal{L}_{SAA}(x; \theta_s), \quad (7)$$

where  $t$  is the epoch,  $\eta$  is the learning rate and  $\mathcal{B}$  means the mini-batch samples.

### 3.3. A Close Look at SAA

To verify whether SAA significantly improves the spatial and adversarial features after model alignment, we conduct

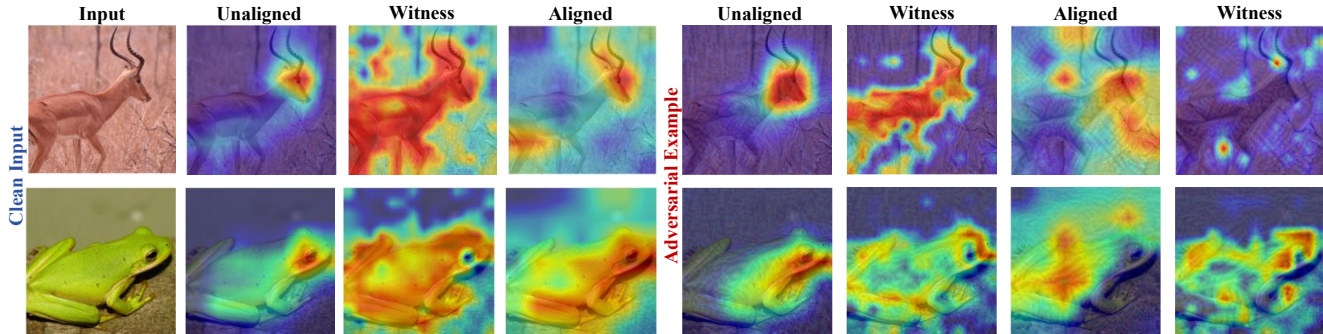


Figure 2. Grad-CAM visualizations comparing the feature distribution of unaligned and aligned surrogate models (Res50) on clean inputs and adversarial examples (generated by SSA-DI-TI-MI).

Table 1. Cosine similarity of global features of surrogate models.

Surrogate	Witness	Clean		Adv	
		Unaligned	Aligned	Unaligned	Aligned
Res50	Res50	<b>1.0000</b>	0.9949	<b>1.0000</b>	0.9922
	DN121	0.0573	<b>0.1153</b>	0.0700	<b>0.1328</b>
	ViT-B	0.0533	<b>0.1408</b>	0.0452	<b>0.1191</b>
	Swin-B	0.0352	<b>0.0448</b>	0.0369	<b>0.0551</b>
ViT-B	Res50	0.0566	<b>0.1323</b>	0.0672	<b>0.1544</b>
	DN121	0.4016	<b>0.6278</b>	0.4121	<b>0.6551</b>
	ViT-B	<b>1.0000</b>	0.9706	<b>1.0000</b>	0.9728
	Swin-B	0.3058	<b>0.5115</b>	0.3169	<b>0.4257</b>

quantitative and qualitative analyses based on the models before and after alignment. We randomly sample 100 images from ImageNet val and then compute the cosine similarity between the global features of the surrogate models before and after applying SAA with different witness models. Table 1 demonstrates that, whether for clean images or adversarial examples (generated by SSA-DI-TI-MI), the feature similarity improves after alignment. Notably, when the surrogate model is ViT-B, the improvement in similarity is even more pronounced. This result suggests that, after applying SAA, the aligned surrogate models effectively capture features shared with the witness model, providing strong evidence of the alignment’s success.

Then, we use Grad-CAM [32]’s heatmaps to simulate the feature distribution of the model, as shown as Figure 2. For the **clean inputs** (first four cols), the heatmaps generated by the unaligned surrogate model (2-nd col) primarily focus on local regions of the object. In contrast, the aligned surrogate model (4-th col) heatmaps demonstrate more diffuse attention spread across the entire object, similar to that of the witness model (ViT-B, 3-rd col), which shows aligned surrogate models learn the common spatial features. For **adversarial examples** (last four cols), the 5-th and 7th cols display the heatmaps of adversarial examples generated by the unaligned and aligned surrogate models, respectively. The 6-th and 8-th show the witness model’s responses to these adversarial examples. Notably,

the adversarial examples generated by the unaligned surrogate model fail to effectively transfer to the witness model (6-th col) due to still focusing on the target subject, indicating limited cross-model transferability. In contrast, adversarial examples generated by the aligned surrogate model (7-th col) successfully transferred to the witness model (8-th col) as the features are spread out, demonstrating enhanced cross-model transferability achieved through SAA.

## 4. Experiments

### 4.1. Experimental Setup

**Datasets.** Our experiments utilize the ImageNet-compatible dataset [21], a widely adopted subset containing 1,000 images from the ImageNet validation set [7]. This dataset is commonly used in adversarial robustness studies, such as those in [9, 10, 45].

**Models.** To assess the adversarial transferability of different network architectures, we focus on convolutional neural networks (CNNs) and vision transformers (ViTs) as the target models. For CNNs, we select the typically trained ResNet-18 (Res18), ResNet-50 (Res50) and ResNet-101 (Res101) [16], VGG-19 [33], DenseNet-121 (DN121) [19], and Inception-v3 (Inc-v3) [35]. For ViTs, we evaluate the Vision Transformer (ViT-B) [11], Swin Transformer (Swin-B) [24], Pyramid Vision Transformer (PVT-v2) [38], and MobileViT-s (MobViT) [28].

**Metric.** Adversarial transferability is quantified by calculating the average attack success rate (Avg. ASR, %) across target models (excluding the surrogate model), with a higher success rate signifying enhanced transferability. In the paper, ‘n/a’ is defined as the average attack success rate obtained by generating adversarial examples using the surrogate model without any alignment, serving as a baseline.

**Implementation Details.** In our experiments, we select the MI [9] attack as the baseline for generating adversarial examples with high transferability, as it is widely recognized within the field of adversarial transferability [10, 22, 25, 37, 39, 40, 42–45]. For MI, we set the perturbation magnitude

Table 2. Comparison of adversarial transferability on different alignment methods.

Surrogate	Witness	Attack	Target Model										Avg. ASR (%)
			CNNs						ViTs				
			Res18	Res50	Res101	VGG19	DN121	Inc-v3	ViT-B	Swin-B	PVT-v2	MobViT	
Res50	n/a	MI	57.7	99.9	58.1	54.2	55.1	39.0	9.4	33.0	38.0	35.7	42.2
	Res50	MA	60.4	99.8	56.4	60.3	67.3	44.3	12.1	35.6	37.2	39.0	45.8
		SAA	<b>77.5</b>	<b>100.0</b>	<b>71.7</b>	<b>72.0</b>	<b>77.0</b>	<b>58.7</b>	<b>19.9</b>	<b>47.8</b>	<b>51.8</b>	<b>52.8</b>	<b>58.8</b>
	DN121	MA	83.1	96.7	75.8	82.3	87.1	64.0	19.8	49.6	54.5	59.2	63.9
		SAA	<b>92.4</b>	<b>98.6</b>	<b>87.1</b>	<b>90.3</b>	<b>94.6</b>	<b>77.8</b>	<b>30.5</b>	<b>64.2</b>	<b>69.2</b>	<b>76.5</b>	<b>75.8</b>
	ViT-B	MA	74.2	99.2	63.5	69.3	72.8	51.5	18.5	41.5	42.7	47.4	53.5
SAA		<b>84.1</b>	<b>99.6</b>	<b>74.7</b>	<b>80.3</b>	<b>81.8</b>	<b>65.7</b>	<b>24.3</b>	<b>48.7</b>	<b>52.9</b>	<b>62.5</b>	<b>63.9</b>	
Swin-B	MA	64.7	90.4	50.6	61.2	61.6	42.3	10.7	33.6	36.4	38.8	44.4	
	SAA	<b>79.7</b>	<b>95.7</b>	<b>66.4</b>	<b>74.1</b>	<b>75.9</b>	<b>56.9</b>	<b>19.6</b>	<b>41.9</b>	<b>47.9</b>	<b>55.2</b>	<b>57.5</b>	
DN121	n/a	MI	84.4	69.6	54.8	76.6	100.0	56.5	16.2	42.1	43.9	52.6	58.6
	Res50	MA	88.8	65.8	49.8	78.3	<b>100.0</b>	55.7	14.9	40.0	38.2	53.0	57.6
		SAA	<b>95.7</b>	<b>80.3</b>	<b>70.9</b>	<b>87.7</b>	99.6	<b>78.2</b>	<b>31.4</b>	<b>55.0</b>	<b>56.6</b>	<b>72.1</b>	<b>71.9</b>
	DN121	MA	79.3	69.5	54.9	78.8	<b>100.0</b>	55.4	12.3	39.9	41.7	52.4	57.2
		SAA	<b>90.1</b>	<b>81.4</b>	<b>71.5</b>	<b>87.9</b>	99.9	<b>75.0</b>	<b>25.3</b>	<b>54.9</b>	<b>56.4</b>	<b>69.7</b>	<b>70.1</b>
	ViT-B	MA	89.6	80.6	71.1	88.1	<b>100.0</b>	70.0	22.4	53.9	58.4	68.7	69.1
SAA		<b>94.0</b>	<b>83.6</b>	<b>75.2</b>	<b>90.3</b>	99.8	<b>81.7</b>	<b>27.2</b>	<b>58.0</b>	<b>59.1</b>	<b>80.3</b>	<b>74.0</b>	
Swin-B	MA	88.3	63.9	49.2	77.8	<b>100.0</b>	54.4	14.5	38.1	37.5	52.2	56.9	
	SAA	<b>94.8</b>	<b>80.0</b>	<b>69.1</b>	<b>88.0</b>	99.7	<b>74.4</b>	<b>26.3</b>	<b>50.2</b>	<b>51.6</b>	<b>71.2</b>	<b>69.5</b>	
ViT-B	n/a	MI	48.6	41.0	31.9	58.1	50.8	44.4	100.0	58.1	44.7	47.4	53.8
	Res50	MA	65.8	51.9	43.0	66.9	60.0	51.5	99.7	66.0	57.3	57.6	63.1
		SAA	<b>87.3</b>	<b>80.6</b>	<b>75.9</b>	<b>86.1</b>	<b>87.5</b>	<b>78.0</b>	<b>99.9</b>	<b>91.0</b>	<b>85.4</b>	<b>85.2</b>	<b>86.3</b>
	DN121	MA	88.9	73.6	67.6	89.1	87.8	74.9	<b>100.0</b>	84.9	78.3	82.7	83.8
		SAA	<b>94.7</b>	<b>86.8</b>	<b>81.3</b>	<b>93.8</b>	<b>94.0</b>	<b>86.6</b>	99.8	<b>91.3</b>	<b>87.2</b>	<b>90.7</b>	<b>91.0</b>
	ViT-B	MA	54.3	37.2	29.2	56.0	47.9	42.4	<b>100.0</b>	52.8	42.3	47.4	52.5
SAA		<b>62.7</b>	<b>46.9</b>	<b>40.9</b>	<b>64.2</b>	<b>57.5</b>	<b>52.1</b>	100.0	<b>59.5</b>	<b>52.6</b>	<b>58.8</b>	<b>60.9</b>	
Swin-B	MA	66.6	46.0	38.3	67.5	57.6	50.8	<b>99.7</b>	65.7	53.6	58.2	62.0	
	SAA	<b>83.0</b>	<b>69.2</b>	<b>65.6</b>	<b>81.2</b>	<b>78.1</b>	<b>74.2</b>	99.3	<b>84.3</b>	<b>76.0</b>	<b>78.3</b>	<b>80.0</b>	
Swin-B	n/a	MI	48.2	31.3	20.0	49.3	34.3	29.7	13.9	100.0	45.4	41.4	42.5
	Res50	MA	54.8	50.9	36.5	61.8	49.3	40.1	32.4	<b>100.0</b>	68.5	55.6	55.4
		SAA	<b>90.3</b>	<b>85.3</b>	<b>77.9</b>	<b>92.0</b>	<b>88.4</b>	<b>76.4</b>	<b>64.7</b>	99.9	<b>92.4</b>	<b>89.0</b>	<b>85.7</b>
	DN121	MA	77.3	71.4	60.0	83.9	76.4	60.7	49.0	<b>100.0</b>	85.9	80.9	74.9
		SAA	<b>94.9</b>	<b>91.7</b>	<b>85.8</b>	<b>96.5</b>	<b>94.7</b>	<b>85.6</b>	<b>74.3</b>	<b>100.0</b>	<b>95.5</b>	<b>95.4</b>	<b>91.4</b>
	ViT-B	MA	62.6	52.8	40.0	66.2	55.3	45.6	34.0	<b>100.0</b>	70.1	61.8	59.5
SAA		<b>84.7</b>	<b>80.0</b>	<b>74.2</b>	<b>90.5</b>	<b>85.5</b>	<b>75.7</b>	<b>70.3</b>	<b>100.0</b>	<b>91.9</b>	<b>88.6</b>	<b>84.6</b>	
Swin-B	MA	62.6	52.8	40.0	66.2	55.3	45.6	<b>34.0</b>	<b>100.0</b>	70.1	61.8	59.5	
	SAA	<b>73.5</b>	<b>58.9</b>	<b>45.7</b>	<b>79.2</b>	<b>63.4</b>	<b>50.7</b>	32.8	<b>100.0</b>	<b>75.8</b>	<b>71.4</b>	<b>65.8</b>	

$\epsilon = 16$ , perform 10 iterations, with a step size of  $\frac{16}{10} = 1.6$ , and use a momentum  $\mu = 1$ . During the Spatial Adversarial Alignment, all surrogate models are fine-tuned for one epoch using stochastic gradient descent (SGD) with a momentum of 0.9, and no learning rate adjustments are applied. It is important to note that no additional data is used for fine-tuning, as it relies solely on the same training data used for both the surrogate and witness models. The settings for Model Alignment (MA) [26] are consistent with the parameters specified in the original paper.

## 4.2. Performance Comparison

**Performance comparison with alignment methods.** We first compare with existing alignment methods [26], where

adversarial examples are generated based on MI [9]. Table 2 illustrates the performance difference between MA and SAA in terms of adversarial transferability, with SAA demonstrating a significant advantage over MA. For instance, when the surrogate model is Res50, and the witness model is also Res50, SAA achieves a 16.6% improvement in average ASR over the original surrogate model, compared to a modest 3.6% improvement with MA. This highlights that SAA, even without introducing additional information, enhances adversarial transferability through the alignment of adversarial features. Furthermore, when the witness models are DN121, ViT-B, and Swin-B, SAA outperforms MA by 11.9%, 10.4%, and 13.1%, respectively. In addition to the remarkable adversarial transferability that

Table 3. SAA has stronger adversarial transferability after being compatible with existing transfer attacks.

Attack	Target Model										Avg. ASR (%)
	CNNs						ViTs				
	Res18	Res50	Res101	VGG19	DN121	Inc-v3	ViT-B	Swin-B	PVT-v2	MobViT	
MI	57.7	<b>99.9</b>	58.1	54.2	55.1	39.0	26.3	15.1	38.0	35.7	42.1
MI-SAA	<b>84.1</b>	<b>99.6</b>	<b>74.7</b>	<b>80.3</b>	<b>81.8</b>	<b>65.7</b>	<b>53.1</b>	<b>34.8</b>	<b>52.9</b>	<b>62.5</b>	<b>65.5</b>
NI	58.9	<b>100.0</b>	63.2	59.3	61.4	40.0	27.3	15.2	41.8	38.1	45.0
NI-SAA	<b>86.1</b>	<b>99.9</b>	<b>76.3</b>	<b>82.2</b>	<b>83.7</b>	<b>67.6</b>	<b>53.2</b>	<b>35.6</b>	<b>55.7</b>	<b>64.8</b>	<b>67.2</b>
GI	57.3	<b>100.0</b>	62.3	60.5	60.5	40.7	29.5	17.3	40.7	39.6	45.4
GI-SAA	<b>86.5</b>	99.7	<b>78.8</b>	<b>83.9</b>	<b>84.8</b>	<b>70.4</b>	<b>58.8</b>	<b>39.6</b>	<b>55.8</b>	<b>66.3</b>	<b>69.4</b>
DI	44.1	<b>95.8</b>	41.7	56.1	44.2	26.1	16.5	7.7	36.7	35.1	34.2
DI-SAA	<b>74.6</b>	94.4	<b>61.1</b>	<b>81.1</b>	<b>73.2</b>	<b>53.1</b>	<b>34.9</b>	<b>19.9</b>	<b>50.8</b>	<b>63.6</b>	<b>56.9</b>
TI	38.5	<b>99.9</b>	<b>37.8</b>	33.9	36.1	24.2	16.8	7.9	29.0	21.1	27.3
TI-SAA	<b>59.7</b>	94.9	35.2	<b>50.6</b>	<b>54.5</b>	<b>40.6</b>	<b>29.2</b>	<b>13.6</b>	<b>29.3</b>	<b>33.6</b>	<b>38.5</b>
SSA	75.8	<b>99.9</b>	<b>78.6</b>	76.0	77.8	57.0	35.3	24.1	55.0	50.5	58.9
SSA-SAA	<b>91.5</b>	99.5	77.8	<b>85.7</b>	<b>88.4</b>	<b>74.9</b>	<b>54.4</b>	<b>36.9</b>	<b>57.1</b>	<b>66.0</b>	<b>70.3</b>
DI-MI	65.5	97.0	65.0	74.7	65.7	49.1	34.5	22.1	54.9	57.9	54.4
DI-MI-SAA	<b>91.9</b>	<b>98.7</b>	<b>84.9</b>	<b>94.1</b>	<b>90.5</b>	<b>78.3</b>	<b>64.9</b>	<b>46.2</b>	<b>76.1</b>	<b>86.8</b>	<b>79.3</b>
TI-MI	61.4	<b>99.9</b>	60.5	60.9	60.9	44.3	35.5	19.6	42.3	41.8	47.5
TI-MI-SAA	<b>84.8</b>	99.3	<b>71.9</b>	<b>79.0</b>	<b>81.8</b>	<b>69.1</b>	<b>58.9</b>	<b>38.7</b>	<b>52.8</b>	<b>62.4</b>	<b>66.6</b>
SSA-MI	89.6	<b>99.9</b>	92.2	89.5	91.0	77.6	57.8	49.4	76.4	76.3	77.8
SSA-MI-SAA	<b>96.3</b>	99.8	<b>95.6</b>	<b>96.5</b>	<b>97.2</b>	<b>91.5</b>	<b>81.3</b>	<b>68.2</b>	<b>80.4</b>	<b>88.4</b>	<b>88.4</b>
SSA-DI-TI-MI	93.5	98.5	92.3	95.0	93.7	85.5	78.9	66.5	87.1	89.8	86.9
SSA-DI-TI-MI-SAA	<b>97.5</b>	<b>98.8</b>	<b>93.8</b>	<b>97.6</b>	<b>96.7</b>	<b>94.3</b>	<b>90.6</b>	<b>78.0</b>	<b>84.4</b>	<b>94.7</b>	<b>92.0</b>

Table 4. SAA further improves the adversarial transferability of adversarial attacks on ViTs.

Attack	Target Model										Avg. ASR (%)
	CNNs						ViTs				
	Res18	Res50	Res101	VGG19	DN121	Inc-v3	ViT-B	Swin-B	PVT-v2	MobViT	
SGM	82.9	67.6	59.4	81.2	75.4	71.3	<b>99.7</b>	83.3	72.7	78.8	78.3
SGM-SAA	<b>91.1</b>	<b>79.8</b>	<b>73.3</b>	<b>87.5</b>	<b>87.3</b>	<b>80.9</b>	99.5	<b>90.5</b>	<b>82.6</b>	<b>86.3</b>	<b>86.6</b>
PatchOut	45.6	27.4	20.3	45.5	36.1	33.9	93.0	41.0	34.2	40.5	43.3
PatchOut-SAA	<b>76.5</b>	<b>72.4</b>	<b>70.3</b>	<b>79.4</b>	<b>78.1</b>	<b>71.3</b>	<b>94.7</b>	<b>83.6</b>	<b>77.2</b>	<b>76.8</b>	<b>78.7</b>
PNA	61.2	45.0	38.1	60.8	54.8	49.0	<b>99.6</b>	66.3	55.8	56.8	60.3
PNA-SAA	<b>82.7</b>	<b>78.1</b>	<b>73.4</b>	<b>85.6</b>	<b>84.0</b>	<b>75.1</b>	97.4	<b>89.3</b>	<b>80.3</b>	<b>82.1</b>	<b>83.3</b>
TGR	74.0	55.6	48.4	73.2	66.6	59.0	<b>99.3</b>	74.5	61.6	69.6	69.6
TGR-SAA	<b>85.9</b>	<b>78.1</b>	<b>71.5</b>	<b>87.4</b>	<b>85.6</b>	<b>79.6</b>	<b>99.3</b>	<b>89.1</b>	<b>81.0</b>	<b>86.2</b>	<b>85.1</b>

SAA provides, we make two other key observations: (i) MA only considers global features, which makes it difficult to align features between models with large differences, which may lead to a decrease in transferability. When the surrogate model is DN121 and the witness model is Swin-B, the ASR of ViT-B, Swin-B, PVT-v2, and MobViT is not as good as the origin DN121, which shows that relying solely on global features for alignment is not enough, and can only achieve poor transferability. (ii) SAA provides strong cross-architecture transferability. When the surrogate model is Res50, and the witness models are Res50, DN121, ViT-B, and Swin-B, the transferability of SAA on ViTs is improved by 39.06%, 31.29%, 25.51%, and 37.74% respectively compared with MA itself, and it also has high transferability between CNNs.

**Performance comparison with transfer attacks.** Aligned

surrogate models by SAA have great potential for adversarial transferability, so existing transfer attacks such as advanced optimization and data augmentation can further improve transferability. Here, we choose Res50 as the surrogate model and ViT-B as the witness model, and superimpose them with MI [9], NI [22], GI [37], DI [45], TI [10] and SSA [25] to evaluate the transferability, as shown in Table 3. Taking GI and SSA as examples, the transferability of the model after SAA is improved by 24.0% and 11.4% respectively compared with the origin surrogate model, which is a very significant improvement. When multiple attacks are integrated, such as SSA-DI-TI-MI, SAA further enhances the transferability by 5.1%, achieving an impressive 92.0% ASR, which closely approaches the performance of white-box attacks. This indicates that SAA substantially narrows the performance gap between black-box and white-

Table 5. Ablation study on alignment modules.

Module			Target Model										Avg. ASR (%)
Spatial		Adversarial	CNNs					ViTs					
Global	Local		Res18	Res50	Res101	VGG19	DN121	Inc-v3	ViT-B	Swin-B	PVT-v2	MobViT	
			57.7	<b>99.9</b>	58.1	54.2	55.1	39.0	9.4	33.0	38.0	35.7	42.2
✓			60.4	99.8	56.4	60.3	67.3	44.3	12.1	35.6	37.2	39.0	45.8
✓	✓		67.5	98.0	58.1	69.1	70.1	49.9	12.2	37.7	38.9	47.7	50.1
✓		✓	81.6	97.9	68.1	53.0	79.8	63.6	<b>25.5</b>	47.9	48.7	57.3	58.4
✓	✓	✓	<b>84.1</b>	99.6	<b>74.7</b>	<b>80.3</b>	<b>81.8</b>	<b>65.7</b>	24.3	<b>48.7</b>	<b>52.9</b>	<b>62.5</b>	<b>63.9</b>

box attacks, thereby facilitating a more comprehensive evaluation of the adversarial robustness of existing models.

**Performance comparison with attacks on ViTs.** To further explore the cross-architecture transferability, we evaluate adversarial attacks on ViTs, including SGM [44], PatchOut [43], PNA [43], and TGR [49]. Here, we choose the surrogate model as ViT-B and the witness model as Res50. In PatchOut, SAA first improves the transferability between ViTs, for example, the ASR from ViT-B to Swin-B is improved by 42.6%. Secondly, SAA greatly improves the transferability from ViT to CNN, for example, the ASR is improved by 45.0% and 42.0% on Res50 and DN121 respectively. On SGM, PNA, and TGR, SAA also achieves stronger cross-architecture transferability without modifying the forward and backward propagation of the model.

### 4.3. Ablation Studies

We select ResNet-50 as the surrogate model and ViT-B as the witness model for ablation studies.

**Alignment Module.** In spatial-aware alignment, ‘global’ represents  $\mathcal{L}_{global}$  (Equation 1), while ‘local’ represents  $\mathcal{L}_{local}$  (Equation 2). Similarly, ‘adversarial’ represents  $\mathcal{L}_{AA}$  (Equation 5) of adversarial-aware alignment. As shown in Table 5, when global features are introduced into the alignment, the transferability of the aligned surrogate model will increase by 3.6%. Based on  $\mathcal{L}_{global}$ , when only local features are introduced, the overall transferability is improved by 4.3% due to better alignment of features of different architectures in local regions, especially by 8.7% on MobViT. Based on  $\mathcal{L}_{global}$ , when only adversarial features are introduced, the transferability is greatly improved, reaching 12.6% ASR, and the improvement is significant on ViTs. Finally, by integrating all features, the aligned surrogate model achieves state-of-the-art transferability. Through the above experiments, we illustrate the effectiveness of spatial-aware and adversarial-aware alignment.

**Training Epochs.** In Section 4.2, we reveal the powerful potential of SAA for adversarial transferability after training for only one epoch. Furthermore, we explore the performance difference after training for multiple epochs, as shown in Figure 3. We calculate the average attack success rate except for the Res50 surrogate model itself and find that with the increase of epochs, the adversarial transferability of the aligned surrogate model is further improved, reaching

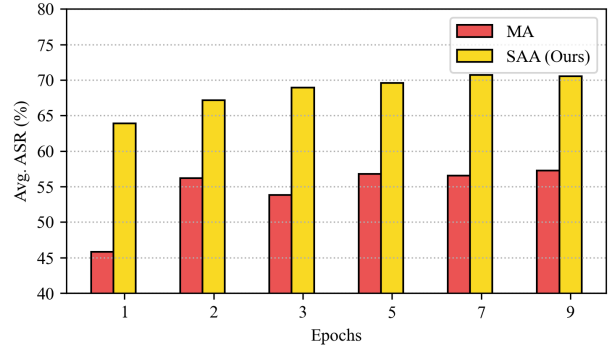


Figure 3. Ablation study on training epochs.

convergence around the 9-th epoch. Compared with MA, SAA can achieve higher transferability in small epochs, and after multiple rounds of training, the transferability has a higher upper limit, which shows the importance of using spatial and adversarial features for model alignment.

## 5. Conclusions

In this study, we introduce a novel technique called Spatial Adversarial Alignment (SAA), which incorporates an alignment loss function and utilizes a witness model to fine-tune a surrogate model by focusing on both spatial-aware and adversarial-aware alignments. Through comprehensive experimental analysis, we demonstrate that leveraging these spatial and adversarial features for model alignment significantly enhances the adversarial transferability of surrogate models, with a particularly pronounced improvement in their cross-architecture capabilities. The proposed SAA method not only integrates seamlessly with existing transfer attack strategies but also further amplifies adversarial transferability, thereby contributing to a more complete evaluation of the adversarial robustness of current DNNs.

**Boarder Impacts.** The adversarial examples generated by surrogate models after the application of SAA exhibit enhanced adversarial transferability, with particularly improved cross-architecture capabilities. This augmented transferability poses a significant threat to the deployment of deep learning models in real-world applications. Additionally, through empirical experiments, we demonstrate the critical role of spatial and adversarial features in improving transferability. While a comprehensive theoretical analysis



is still lacking, these findings highlight the need for further investigation into adversarial robustness and the development of effective defense mechanisms.

## References

- [1] Junyoung Byun, Myung-Joon Kwon, Seungju Cho, Yoonji Kim, and Changick Kim. Introducing competition to boost the transferability of targeted adversarial examples through clean feature mixup. In *IEEE/CVF Conference on Computer Vision and Pattern Recognition, CVPR 2023, Vancouver, BC, Canada, June 17-24, 2023*, pages 24648–24657. IEEE, 2023. 4
- [2] Zhengsu Chen, Lingxi Xie, Jianwei Niu, Xuefeng Liu, Longhui Wei, and Qi Tian. Visformer: The vision-friendly transformer. In *2021 IEEE/CVF International Conference on Computer Vision, ICCV 2021, Montreal, QC, Canada, October 10-17, 2021*, pages 569–578. IEEE, 2021. 3
- [3] Zhaoyu Chen, Bo Li, Shuang Wu, Jianghe Xu, Shouhong Ding, and Wenqiang Zhang. Shape matters: deformable patch attack. In *European Conference on Computer Vision*, pages 529–548. Springer, 2022. 1
- [4] Zhaoyu Chen, Bo Li, Jianghe Xu, Shuang Wu, Shouhong Ding, and Wenqiang Zhang. Towards practical certifiable patch defense with vision transformer. In *Proceedings of the IEEE/CVF Conference on Computer Vision and Pattern Recognition*, pages 15148–15158, 2022.
- [5] Zhaoyu Chen, Bo Li, Shuang Wu, Shouhong Ding, and Wenqiang Zhang. Query-efficient decision-based black-box patch attack. *IEEE Transactions on Information Forensics and Security*, 18:5522–5536, 2023.
- [6] Zhaoyu Chen, Bo Li, Shuang Wu, Kaixun Jiang, Shouhong Ding, and Wenqiang Zhang. Content-based unrestricted adversarial attack. In *Advances in Neural Information Processing Systems*, pages 51719–51733, 2023. 1
- [7] Jia Deng, Wei Dong, Richard Socher, Li-Jia Li, Kai Li, and Fei-Fei Li. Imagenet: A large-scale hierarchical image database. In *CVPR*, pages 248–255, 2009. 5
- [8] Terrance DeVries. Improved regularization of convolutional neural networks with cutout. *arXiv preprint arXiv:1708.04552*, 2017. 2
- [9] Yinpeng Dong, Fangzhou Liao, Tianyu Pang, Hang Su, Jun Zhu, Xiaolin Hu, and Jianguo Li. Boosting adversarial attacks with momentum. In *2018 IEEE Conference on Computer Vision and Pattern Recognition, CVPR 2018, Salt Lake City, UT, USA, June 18-22, 2018*, pages 9185–9193. Computer Vision Foundation / IEEE Computer Society, 2018. 1, 2, 3, 5, 6, 7
- [10] Yinpeng Dong, Tianyu Pang, Hang Su, and Jun Zhu. Evading defenses to transferable adversarial examples by translation-invariant attacks. In *Proceedings of the IEEE/CVF Conference on Computer Vision and Pattern Recognition*, pages 4312–4321, 2019. 1, 2, 3, 4, 5, 7
- [11] Alexey Dosovitskiy, Lucas Beyer, Alexander Kolesnikov, Dirk Weissenborn, Xiaohua Zhai, Thomas Unterthiner, Mostafa Dehghani, Matthias Minderer, Georg Heigold, Sylvain Gelly, Jakob Uszkoreit, and Neil Houlsby. An image is worth 16x16 words: Transformers for image recognition at scale. In *ICLR*, 2021. 1, 5
- [12] F. Croce and M. Hein. Reliable evaluation of adversarial robustness with an ensemble of diverse parameter-free attacks. In *ICML*, pages 2206–2216, 2020. 1
- [13] Ian J. Goodfellow, Jonathon Shlens, and Christian Szegedy. Explaining and harnessing adversarial examples. In *ICLR*, 2015. 1, 2
- [14] Pinxue Guo, Wanyun Li, Hao Huang, Lingyi Hong, Xinyu Zhou, Zhaoyu Chen, Jinglun Li, Kaixun Jiang, Wei Zhang, and Wenqiang Zhang. X-prompt: Multi-modal visual prompt for video object segmentation. In *Proceedings of the 32nd ACM International Conference on Multimedia*, pages 5151–5160, 2024. 1
- [15] Yiwen Guo, Qizhang Li, and Hao Chen. Backpropagating linearly improves transferability of adversarial examples. In *Advances in Neural Information Processing Systems 33: Annual Conference on Neural Information Processing Systems 2020, NeurIPS 2020, December 6-12, 2020, virtual*, 2020. 1, 2
- [16] Kaiming He, Xiangyu Zhang, Shaoqing Ren, and Jian Sun. Deep residual learning for image recognition. In *CVPR*, pages 770–778, 2016. 1, 5
- [17] Lingyi Hong, Wenchao Chen, Zhongying Liu, Wei Zhang, Pinxue Guo, Zhaoyu Chen, and Wenqiang Zhang. Lvos: A benchmark for long-term video object segmentation. In *Proceedings of the IEEE/CVF International Conference on Computer Vision*, pages 13480–13492, 2023. 1
- [18] Lingyi Hong, Shilin Yan, Renrui Zhang, Wanyun Li, Xinyu Zhou, Pinxue Guo, Kaixun Jiang, Yiting Chen, Jinglun Li, Zhaoyu Chen, et al. Onetracker: Unifying visual object tracking with foundation models and efficient tuning. In *Proceedings of the IEEE/CVF Conference on Computer Vision and Pattern Recognition*, pages 19079–19091, 2024. 1
- [19] Gao Huang, Zhuang Liu, Laurens van der Maaten, and Kilian Q. Weinberger. Densely connected convolutional networks. In *CVPR*, pages 2261–2269, 2017. 5
- [20] Alexey Kurakin, Ian J Goodfellow, and Samy Bengio. Adversarial examples in the physical world. In *Artificial intelligence safety and security*, pages 99–112. Chapman and Hall/CRC, 2018. 2
- [21] Alexey Kurakin, Ian J Goodfellow, and Samy Bengio. Adversarial examples in the physical world. In *Artificial intelligence safety and security*, pages 99–112. Chapman and Hall/CRC, 2018. 5
- [22] Jiadong Lin, Chuanbiao Song, Kun He, Liwei Wang, and John E. Hopcroft. Nesterov accelerated gradient and scale invariance for adversarial attacks. In *8th International Conference on Learning Representations, ICLR 2020, Addis Ababa, Ethiopia, April 26-30, 2020*. OpenReview.net, 2020. 1, 2, 5, 7
- [23] Yanpei Liu, Xinyun Chen, Chang Liu, and Dawn Song. Delving into transferable adversarial examples and black-box attacks. In *5th International Conference on Learning Representations, ICLR 2017, Toulon, France, April 24-26, 2017, Conference Track Proceedings*. OpenReview.net, 2017. 2

- [24] Ze Liu, Yutong Lin, Yue Cao, Han Hu, Yixuan Wei, Zheng Zhang, Stephen Lin, and Baining Guo. Swin transformer: Hierarchical vision transformer using shifted windows. In *ICCV*, pages 9992–10002, 2021. 5
- [25] Yuyang Long, Qilong Zhang, Boheng Zeng, Lianli Gao, Xi-anlong Liu, Jian Zhang, and Jingkuan Song. Frequency domain model augmentation for adversarial attack. In *European Conference on Computer Vision*, 2022. 1, 2, 4, 5, 7
- [26] Avery Ma, Amir-massoud Farahmand, Yangchen Pan, Philip Torr, and Jindong Gu. Improving adversarial transferability via model alignment. In *European Conference on Computer Vision*, pages 74–92. Springer, 2025. 2, 3, 6
- [27] Aleksander Madry, Aleksandar Makelov, Ludwig Schmidt, Dimitris Tsipras, and Adrian Vladu. Towards deep learning models resistant to adversarial attacks. In *ICLR*, 2018. 1
- [28] Sachin Mehta and Mohammad Rastegari. Mobilevit: Lightweight, general-purpose, and mobile-friendly vision transformer. In *The Tenth International Conference on Learning Representations, ICLR 2022, Virtual Event, April 25-29, 2022*, 2022. 5
- [29] Muzammal Naseer, Kanchana Ranasinghe, Salman Khan, Fahad Shahbaz Khan, and Fatih Porikli. On improving adversarial transferability of vision transformers. In *The Tenth International Conference on Learning Representations, ICLR 2022, Virtual Event, April 25-29, 2022*. OpenReview.net, 2022. 3
- [30] Weili Nie, Brandon Guo, Yujia Huang, Chaowei Xiao, Arash Vahdat, and Anima Anandkumar. Diffusion models for adversarial purification. In *International Conference on Machine Learning (ICML)*, 2022. 4
- [31] Zeyu Qin, Yanbo Fan, Yi Liu, Li Shen, Yong Zhang, Jue Wang, and Baoyuan Wu. Boosting the transferability of adversarial attacks with reverse adversarial perturbation. In *Advances in Neural Information Processing Systems 35: Annual Conference on Neural Information Processing Systems 2022, NeurIPS 2022, New Orleans, LA, USA, November 28 - December 9, 2022*, 2022. 2
- [32] Ramprasaath R. Selvaraju, Michael Cogswell, Abhishek Das, Ramakrishna Vedantam, Devi Parikh, and Dhruv Batra. Grad-cam: Visual explanations from deep networks via gradient-based localization. *Int. J. Comput. Vis.*, 128(2):336–359, 2020. 5
- [33] Karen Simonyan and Andrew Zisserman. Very deep convolutional networks for large-scale image recognition. In *ICLR*, 2015. 5
- [34] Zhimin Sun, Shen Chen, Taiping Yao, Ran Yi, Shouhong Ding, and Lizhuang Ma. Rethinking open-world deepfake attribution with multi-perspective sensory learning. *International Journal of Computer Vision*, 2024. 1
- [35] Christian Szegedy, Vincent Vanhoucke, Sergey Ioffe, Jonathon Shlens, and Zbigniew Wojna. Rethinking the inception architecture for computer vision. In *2016 IEEE Conference on Computer Vision and Pattern Recognition, CVPR 2016, Las Vegas, NV, USA, June 27-30, 2016*, pages 2818–2826, 2016. 5
- [36] Hugo Touvron, Matthieu Cord, Alexandre Sablayrolles, Gabriel Synnaeve, and Hervé Jégou. Going deeper with image transformers. In *2021 IEEE/CVF International Conference on Computer Vision, ICCV 2021, Montreal, QC, Canada, October 10-17, 2021*, pages 32–42. IEEE, 2021. 3
- [37] Jiafeng Wang, Zhaoyu Chen, Kaixun Jiang, Dingkan Yang, Lingyi Hong, Pinxue Guo, Haijing Guo, and Wenqiang Zhang. Boosting the transferability of adversarial attacks with global momentum initialization. *Expert Systems with Applications*, 255:124757, 2024. 1, 2, 5, 7
- [38] Wenhai Wang, Enze Xie, Xiang Li, Deng-Ping Fan, Kaitao Song, Ding Liang, Tong Lu, Ping Luo, and Ling Shao. PVT v2: Improved baselines with pyramid vision transformer. *Comput. Vis. Media*, 8(3):415–424, 2022. 5
- [39] Xiaosen Wang and Kun He. Enhancing the transferability of adversarial attacks through variance tuning. In *IEEE Conference on Computer Vision and Pattern Recognition, CVPR 2021, virtual, June 19-25, 2021*, pages 1924–1933. Computer Vision Foundation / IEEE, 2021. 2, 5
- [40] Xiaosen Wang, Xuanran He, Jingdong Wang, and Kun He. Admix: Enhancing the transferability of adversarial attacks. In *Proceedings of the IEEE/CVF International Conference on Computer Vision*, pages 16158–16167, 2021. 2, 5
- [41] Xiaosen Wang, Kangheng Tong, and Kun He. Rethinking the backward propagation for adversarial transferability. In *Advances in Neural Information Processing Systems 36: Annual Conference on Neural Information Processing Systems 2023, NeurIPS 2023, New Orleans, LA, USA, December 10 - 16, 2023*, 2023. 2
- [42] Xiaosen Wang, Zeliang Zhang, and Jianping Zhang. Structure invariant transformation for better adversarial transferability. In *Proceedings of the IEEE/CVF International Conference on Computer Vision (ICCV)*, pages 4607–4619, 2023. 5
- [43] Zhipeng Wei, Jingjing Chen, Micah Goldblum, Zuxuan Wu, Tom Goldstein, and Yu-Gang Jiang. Towards transferable adversarial attacks on vision transformers. In *Thirty-Sixth AAAI Conference on Artificial Intelligence, AAAI 2022, Thirty-Fourth Conference on Innovative Applications of Artificial Intelligence, IAAI 2022, The Twelfth Symposium on Educational Advances in Artificial Intelligence, EAAI 2022 Virtual Event, February 22 - March 1, 2022*, pages 2668–2676. AAAI Press, 2022. 1, 2, 3, 8
- [44] Dongxian Wu, Yisen Wang, Shu-Tao Xia, James Bailey, and Xingjun Ma. Skip connections matter: On the transferability of adversarial examples generated with resnets. In *8th International Conference on Learning Representations, ICLR 2020, Addis Ababa, Ethiopia, April 26-30, 2020*. OpenReview.net, 2020. 1, 2, 8
- [45] Cihang Xie, Zhishuai Zhang, Yuyin Zhou, Song Bai, Jianyu Wang, Zhou Ren, and Alan L Yuille. Improving transferability of adversarial examples with input diversity. In *Proceedings of the IEEE/CVF Conference on Computer Vision and Pattern Recognition*, pages 2730–2739, 2019. 1, 2, 3, 5, 7
- [46] Dingkan Yang, Shuai Huang, Zhi Xu, Zhenpeng Li, Shunli Wang, Mingcheng Li, Yuzheng Wang, Yang Liu, Kun Yang, Zhaoyu Chen, et al. Aide: A vision-driven multi-view, multi-modal, multi-tasking dataset for assistive driving perception. In *Proceedings of the IEEE/CVF International Conference on Computer Vision*, pages 20459–20470, 2023. 1

- [47] Xiao Yang, Yinpeng Dong, Tianyu Pang, Hang Su, and Jun Zhu. Boosting transferability of targeted adversarial examples via hierarchical generative networks. In *Computer Vision - ECCV 2022 - 17th European Conference, Tel Aviv, Israel, October 23-27, 2022, Proceedings, Part IV*, pages 725–742. Springer, 2022. 4
- [48] Hongyi Zhang, Moustapha Cissé, Yann N. Dauphin, and David Lopez-Paz. mixup: Beyond empirical risk minimization. In *6th International Conference on Learning Representations, ICLR 2018, Vancouver, BC, Canada, April 30 - May 3, 2018, Conference Track Proceedings*. OpenReview.net, 2018. 2
- [49] Jianping Zhang, Yizhan Huang, Weibin Wu, and Michael R. Lyu. Transferable adversarial attacks on vision transformers with token gradient regularization. In *IEEE/CVF Conference on Computer Vision and Pattern Recognition, CVPR 2023, Vancouver, BC, Canada, June 17-24, 2023*, pages 16415–16424. IEEE, 2023. 3, 8
- [50] Jingyu Zhang, Kun Yang, Hanqi Wang, Peng Sun, and Liang Song. Efficient vehicular collaborative perception based on spatio-temporal feature compression. *IEEE Transactions on Vehicular Technology*, 2024. 1
- [51] Jingyu Zhang, Kun Yang, Yilei Wang, Hanqi Wang, Peng Sun, and Liang Song. Ermvp: Communication-efficient and collaboration-robust multi-vehicle perception in challenging environments. In *Proceedings of the IEEE/CVF Conference on Computer Vision and Pattern Recognition (CVPR)*, pages 12575–12584, 2024. 1
- [52] Tianyi Zheng, Bo Li, Shuang Wu, Ben Wan, Guodong Mu, Shice Liu, Shouhong Ding, and Jia Wang. MFAE: masked frequency autoencoders for domain generalization face anti-spoofing. *IEEE Trans. Inf. Forensics Secur.*, 19:4058–4069, 2024. 1
- [53] Tianyi Zheng, Qinji Yu, Zhaoyu Chen, and Jia Wang. Famim: A novel frequency-domain augmentation masked image model framework for domain generalizable face anti-spoofing. In *ICASSP 2024 - 2024 IEEE International Conference on Acoustics, Speech and Signal Processing (ICASSP)*, pages 4470–4474, 2024. 1
- [54] Xinyu Zhou, Pinxue Guo, Lingyi Hong, Jinglun Li, Wei Zhang, Weifeng Ge, and Wenqiang Zhang. Reading relevant feature from global representation memory for visual object tracking. In *Advances in Neural Information Processing Systems*, pages 10814–10827, 2023. 1